

Sub-shot noise sensitivity via deformed four-headed kitten states

Naeem Akhtar,¹ Xiaosen Yang,^{1,*} Jia-Xin Peng,^{2,†} Inaam Ul Haq,³ Yuee Xie,¹ and Yuanping Chen^{1,‡}

¹*Department of Physics, Jiangsu University, Zhenjiang, 212013, China*

²*School of Physics and Technology, Nantong University, Nantong, 226019, China*

³*Department of Physics, COMSATS University Islamabad, Islamabad Campus, 45550, Pakistan*

(Dated: September 17, 2024)

The original compass state, created by superposing four coherent states, yields anisotropic sub-Planck structures and demonstrates enhanced sensitivity to perturbations, offering advantages for quantum sensing. We propose two variants of this compass state by simultaneously applying photon addition and subtraction in different orders: one with addition first and one with subtraction first to the state. Our variants display sub-Planck structures and improved sensitivity to displacements, with photon addition and subtraction influencing these characteristics. In our cases, adding photons increases the average photon number, while photon subtraction lowers it in the first case and has no effect in the second. Furthermore, an increment in the added number of photons uniformly reduces the size of sub-Planck structures, whereas increasing the number of photons subtracted from the state causes these sub-Planck structures to expand in size; higher photon addition improves sensitivity, while photon subtraction decreases it. Remarkably, under optimal parameters, our specific variants achieve isotropic sub-Planck structures and provide isotropic enhanced sensitivity across all directions, surpassing compass states.

I. INTRODUCTION

Coherent states were first introduced by Schrödinger in 1926 [1, 2], and the concept was further developed in quantum optics by Glauber in 1963 [3]. Quantum superposition phenomena have been intensively investigated within the framework of the harmonic oscillator, leading to the creation of intriguing quantum states [4, 5]. Non-classical nature of such states is revealed through non-classical phase-space features, often visualized using the Wigner function [6, 7], and these states are considered valuable resources for continuous variable (CV) quantum information processing [8–12]. Notably, the macroscopic cat state [13, 14], which is the superposition of two distinct coherent states, is a prominent example of a non-classical quantum state. The notion has been evolved to a generalized form of macroscopic cat states [11, 15–17]. A noteworthy example is the compass state [17], a concept that was introduced by Zurek in 2001. This state exhibits fascinating nonclassical phase-space features at scales significantly smaller than the Planck scale [18, 19]. These sub-Planck scale structures are critically significant due to their capacity to substantially increase sensitivity against displacement [20, 21]. The remarkable enhancement in displacement sensitivity afforded by compass states underscore their potential for advancing quantum measurement techniques and improving the performance of quantum technologies [22].

Both theoretical [23–26] and experimental [27–30] approaches have been employed to generate catlike states. Adding or subtracting photons is the key process by which matter interacts with light, allowing the creation

of unique nonclassical states of light in experiments [31]. It has been demonstrated that applying photon addition and/or subtraction to squeezed-vacuum states may yield quantum states having phase-space features resembling those of a cat state, thereby providing an alternative approach for generating catlike states [32–35]. Photon addition and subtraction have been performed simultaneously in different sequences on a coherent state [36–38]. These deformed coherent states may hold nonclassical and non-Gaussian phase-space characteristics that distinguish them from ordinary coherent states.

Compass states have been explored in different contexts [16, 39–51], and our analysis primarily focuses on the Zurek compass state [17]. This state is notable for their anisotropic sub-Planck phase-space structures and exhibits anisotropic enhanced sensitivity to displacements. In this work, we present variants of this compass state by applying photon addition and subtraction operations simultaneously in different sequences, resulting in various cases. Alternatively, our proposed quantum states can also be considered as a superposition of four deformed coherent states, exhibiting phase-space features similar to those of the original compass state. Our investigation employs a comprehensive phase-space formalism [7], incorporating Wigner function analysis and photon number distribution. Additionally, we also examine the sensitivity to displacements for each case [52, 53] and provide a detailed discussion of the physical significance and implications associated with each scenario. By optimizing the associated parameters, a number of our proposed cases may achieve improved phase-space characteristics relative to the compass state; that is, these cases contain isotropic versions of the sub-Planck structures, and the sensitivity enhancement is also isotropic.

Our analysis is structured as follows: §II covers the basics of sub-Planck structures and their sensitivity to displacement, illustrated with the Zurek compass state.

* yangxs@ujs.edu.cn

† 18217696127@163.com

‡ chenyp@ujs.edu.cn

§III discusses deformed coherent states and our proposed quantum states, offering a detailed analysis. §IV discusses the physical basis and implications of our findings and provides a summary of our discussion.

II. SENSING OF DISPLACEMENTS

The quantum uncertainty principle for position and momentum, expressed through the commutation relation $[\hat{x}, \hat{p}] := i\hbar$ with \hat{x} and \hat{p} being the position and momentum operators, respectively, imposes constraints on the phase-space structure. Specifically, it dictates that the product of the uncertainties in position (Δx) and momentum (Δp) must satisfy the inequality $\Delta x \Delta p \geq \hbar/2$ [18, 19]. The coherent state is known as the minimal uncertainty state [54], but a quantum state may also exhibit phase-space features that fall below the uncertainty limit and named as sub-Planck scale structures. The sensitivity to phase-space displacement of a quantum state may also be connected to the smallest scale of its phase-space structure [21]. For example, the Zurek compass state [17] holds sub-Planck structures in phase space, which enhance its sensitivity beyond standard limits. This implies that the metrological capacity of a quantum state in certain situations may also link to its smallest phase-space structure. This connection will be examined in detail in this section, with a particular focus on the Zurek compass state as a primary example.

A. Phase Space and Sensitivity

A Schrödinger coherent state can be expressed as a displaced vacuum state $|\alpha\rangle := \hat{D}(\alpha)|0\rangle$ with $\hat{D}(\alpha) := \exp(\alpha\hat{a}^\dagger - \alpha^*\hat{a})$ is the displacement operator [55], where $\alpha \in \mathbb{C}$, and \hat{a} (\hat{a}^\dagger) are annihilation (creation) operators. Coherent states are the most classical pure states of light [54], but their superposition may exhibit nonclassical aspects due to quantum interference [56]. The Wigner function denoted by $W_{\hat{\rho}}(\boldsymbol{\beta})$ with $\boldsymbol{\beta} := (x, p)^\top$ constitutes phase space of a quantum state $\hat{\rho}$ [7], where x and p are the position and momentum pairs, respectively.

The Wigner function is one of the primary tools for analyzing the nonclassical characteristics of a quantum state [7]. Mathematically, the Wigner function can also be expressed as [57]

$$W_{\hat{\rho}}(\boldsymbol{\beta}) := \frac{e^{2|\beta|^2}}{\pi^2} \int d^2\gamma \langle -\gamma | \hat{\rho} | \gamma \rangle e^{-2(\beta^* \gamma - \beta \gamma^*)}. \quad (1)$$

Note that dimensionless versions of the position and momentum operators are employed throughout this work.

The Schrödinger cat state is the superposition of two distinguishable coherent states, and one of the simplest examples of such states is the even cat state [58], which

is denoted as

$$|\psi\rangle := \frac{1}{(2 + 2e^{-2|\alpha|^2})^{1/2}} [|\alpha\rangle + |-\alpha\rangle]. \quad (2)$$

A cat state is visible when the parameter α is high enough to maintain the orthogonality criterion $\langle \alpha | -\alpha \rangle \approx 0$. If the constituent coherent states in this superposition are not distinguishable, the resulting states could be called Schrödinger-kitten states [34]. The compass state [17] is an extended and generalized form of this superposition, and can be considered a type of multi-component cat state [15, 59–61], and may also appear in different forms [16, 47–49].

Let us now discuss the concept of sensitivity to phase-space displacement. For a pure quantum state $|\psi\rangle$, this sensitivity can be mathematically determined by evaluating the overlap function between a quantum state and its slightly displaced version. This involves calculating how much one state resembles another when displaced in phase space, which provides insight into how precisely the quantum state can detect or respond to changes in its phase-space configuration. Mathematically, this sensitivity can be determined by using [52]

$$S_{|\psi\rangle}(\delta) := \int \frac{d^2\beta}{\pi} W_{|\psi\rangle}(\beta) W_{|\psi'\rangle}(\beta) = |\langle \psi | \psi' \rangle|^2 \quad (3)$$

with $|\psi'\rangle := \hat{D}(\delta)|\psi\rangle$. If $S_{|\psi\rangle}(\delta) = 0$, then a state and its displaced counterpart are orthogonal for the displacement δ . The overlap $S_{|\psi\rangle}(\delta)$ with $\delta := (\delta x, \delta p)^\top$, where δx and δp are values of the displacements applied along x and p directions in the phase space, respectively. The infinitesimal perturbation δ , which makes the perturbed state quasi-orthogonal with the initial, provides information on the sensitivity to displacements. Smaller values of δ indicate greater sensitivity to displacements. This concept can be understood by considering a scenario where a signal intended for detection is linearly coupled to a harmonic oscillator. The oscillator measures a displacement that is proportional to the strength of the signal. In this context, the sensitivity of the oscillator to these displacements directly impacts its capacity to resolve the signal. Thus, quantum states with higher sensitivity are capable of detecting weaker signals with greater precision [21].

The phase-space structure and sensitivity to displacement of coherent states are at the standard limits, also known as shot noise limit [20]. The Wigner function of a macroscopic cat state typically manifests as two distinct Gaussian peaks in phase space with an oscillatory interference pattern, where each peak corresponds to a coherent state; this configuration may also be termed as a two-headed cat state [61, 62]. In contrast, for a compass state, the Wigner function now holds four Gaussian peaks, catlike interference pattern and a super oscillatory pattern that reveals sub-Planck structures [17], may also be classified as a four-component cat state [60, 61], aligning with the concept of multichotomous cat states [15].

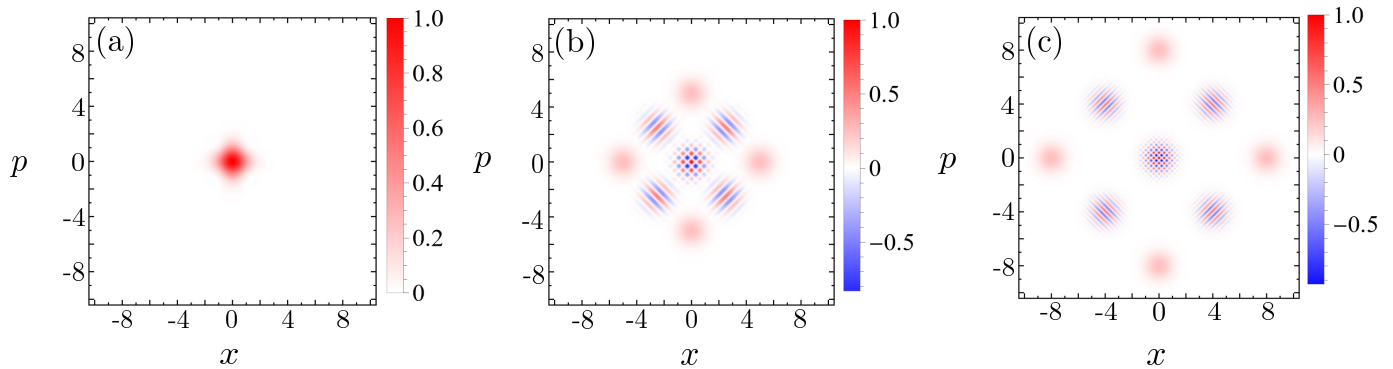


FIG. 1. The Wigner function of the compass state. (a) $c_0 = 1$, (b) $c_0 = 5$, and (c) $c_0 = 8$.

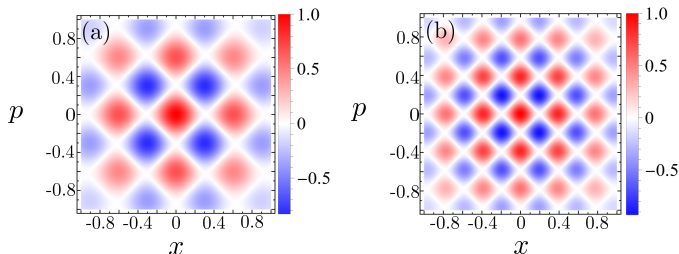


FIG. 2. Central interference of the compass state. (a) $c_0 = 5$ and (b) $c_0 = 8$.

Cat states, such as the one presented in Eq. (2), do not exhibit sub-Planck features as their interference phase-space attributes are not limited in all directions of phase space [47]. Different flavors of the compass states, as introduced in [16, 47–49], hold sub-Planck structures. Their sensitivity against displacement is also enhanced compared to the standard limits, thereby retaining sub-shot noise sensitivity [20]. We review these concepts with details next.

B. Near-isotropic Sub-Planckness

Nonclassical effects in the Wigner function of a quantum system can give rise to remarkable phase-space structures, and these distinctive features play a significant role in enhancing sensitivity to phase-space displacements, a useful concept have been employed in quantum measurements [20, 21]. We now explore this concept through specific examples.

As an example, let us first examine the Wigner function of a coherent state, that is,

$$W_{|\alpha\rangle}(\beta) := e^{-2(\alpha-\beta)(\alpha^*-\beta^*)}, \quad (4)$$

which exhibits Gaussian form; hence, coherent states are types of Gaussian and nonclassical quantum states [54]. Moreover, the phase-space structure of a coherent state follows the minimal limit set by the uncertainty principle,

often referred to as the Planck action in phase space. This implies that phase-space size of a coherent sets the minimal norm, and the sub-Planck structure is below this limit and can be limited as much as desired by varying the controlling parameter, whereas all of these characteristics are missing in the coherent [47].

The sensitivity of a coherent state to displacements in phase space is described by the function $S_{|\alpha\rangle}(\delta) := e^{-|\delta|^2}$. This overlap tends to zero for the displacement $|\delta| > 1$, implying that the sensitivity of a coherent state falls at the standard limits. The phase-space structure of a coherent state and its sensitivity adhere precisely to the standard quantum mechanical limits. This means that the coherent state achieves the theoretical minimum uncertainty allowed by the Heisenberg uncertainty principle, reflecting the optimal balance between precision in position and momentum measurements. Consequently, in our analysis, we evaluate each example by comparing it against these established norms. This involves assessing how each example measures up to the theoretical benchmarks and standard limits, allowing us to understand their relative performance and behavior in relation to these reference points.

Let us now include the example of the Zurek compass state [17], which is recognized as a superposition of coherent states given by $\alpha_1 = c_0/\sqrt{2}$, $\alpha_2 = -c_0/\sqrt{2}$, $\alpha_3 = ic_0/\sqrt{2}$, and $\alpha_4 = -ic_0/\sqrt{2}$, with $c_0 \in \mathbb{R}^+$. This superposition can also be interpreted as the superposition of two cat states, or equivalently as the superposition of four coherent states and is denoted as

$$|\diamond\rangle := N_{\diamond}^{-1/2} \sum_{i=1}^4 |\alpha_i\rangle, \quad (5)$$

where

$$N_{\diamond} = \sum_{i,j=1}^4 G_{\alpha_i, \alpha_j} e^{\alpha_i^* \alpha_j} \quad (6)$$

with

$$G_{k,l} := \exp \left[-\frac{1}{2} \{ |k|^2 + |l|^2 \} \right] \quad (7)$$

represents the normalization coefficient.

The Wigner function of the compass state $|\diamond\rangle$ is obtained as

$$W_{|\diamond\rangle}(\beta) = \frac{1}{N_\diamond} \sum_{i,j=1}^4 W_{|\alpha_i\rangle\langle\alpha_j|}(\beta) \quad (8)$$

with

$$W_{|\alpha_i\rangle\langle\alpha_j|}(\beta) := G_{\alpha_i,\alpha_j} \exp \left[-\alpha_i\alpha_j^* - 2(|\beta|^2 - \alpha_i^*\beta - \alpha_j\beta^*) \right]. \quad (9)$$

We present $W_{|\diamond\rangle}(\beta)$ in Fig. 1 for a few c_0 values. As depicted in Fig. 1(a), for $c_0 = 1$, the four coherent states in the compass state cannot be distinguished individually; hence, the corresponding Wigner distribution shows a central positive peak. This scenario represents the four-component kitten state, or alternatively may also be referred to as a four-headed kitten state [61]. However, for $c_0 = 5$, these four coherent states are now well separated and appear as four Gaussian lobes in the phase space, and the interference pattern is now pronounced in the phase space, as shown in Fig. 1(b). Figure 1(c) shows that increasing the macroscopic parameter to $c_0 = 8$ causes coherent states to be pushed further away from the phase-space origin, resulting in enhanced negative regions in the intensity plot. Figure 2 illustrates the central interference pattern of each case presented in Fig. 1, where the phase-space features are arranged in a tiled format. Each tile in this pattern has an extension considerably smaller than that of a coherent state, indicating that these structures are at the sub-Planck scale. Furthermore, as c_0 increases, the size of the sub-Planck features decreases. These tile-shaped sub-Planck structures highlight their anisotropic properties, contrasting with an isotropic configuration where uniformity in all directions would be expected.

The enhancement in sensitivity for a cat state is limited to a particular direction in the phase space. Consequently, compass states are deemed more advantageous than cat states as they may offer greater sensitivity [47]. The overlap between the compass state $|\diamond\rangle$ and its displaced version $\hat{D}(\delta)|\diamond\rangle$ reflects the sensitivity to displacement in phase space

$$S_\diamond(\delta) = \left| \sum_{i,j=1}^4 O_{|\alpha_i\rangle\langle\alpha_j|}(\delta) \right|^2, \quad (10)$$

where

$$O_{|\alpha_i\rangle\langle\alpha_j|}(\delta) := G_{\alpha_i,\alpha_j} \exp \left[\alpha_i^*\alpha_j + \alpha_i^*\delta - \alpha_j\delta^* - \frac{|\delta|^2}{2} \right]. \quad (11)$$

Note that we skip normalization for the sensitivity cases as their intensity visualizations are already normalized to unity. Figures 2(a) and (b) show that the overlap function $S_\diamond(\delta)$ is zero for $|\delta| < 1$, with $c_0 = 5$ and $c_0 = 8$ in

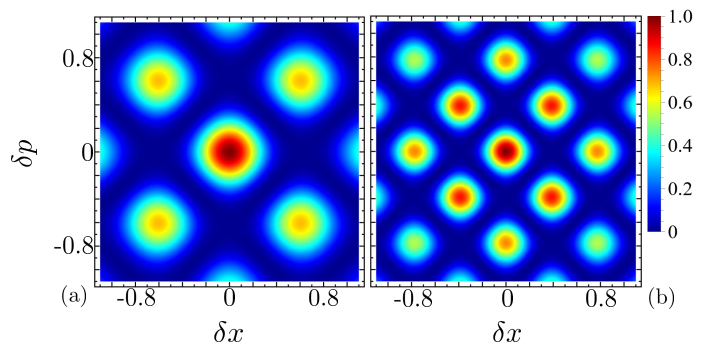


FIG. 3. The overlap between the compass state and its displaced versions, represented by $S_\diamond(\delta)$, quantifies the corresponding sensitivities over given parameters chosen with (a) $c_0 = 5$ and (b) $c_0 = 8$. The intensity plots are normalized to unity for each case.

the respective cases involving the sub-Planck structures. This means that the sensitivity to displacement for this compass state is enhanced as compared to a coherent state. Furthermore, compared to the coherent state, the overlap function is now dependent on c_0 . Raising this parameter causes the overlap function to be zero for smaller values of $|\delta|$, indicating increased sensitivity to displacement compared to coherent states. Generally, the sensitivity of a coherent state $|\alpha\rangle$ is independent of the specific value of α , which relates to the average photon number by $|\alpha|^2$. Consequently, increasing the average photon number does not enhance the sensitivity of a coherent state to displacements, which is solely limited by the shot noise introduced by vacuum fluctuations [54].

In summary, considering the compass state under consideration, sensitivity to displacement appears to be associated to the macroscopic parameter c_0 ; as c_0 grows, it increases both sensitivity and the average photon number in the state. This suggests that a compass state with a larger average photon number can have greater susceptibility to displacement. Furthermore, in this example, the sensitivity to displacement is anisotropically amplified, as illustrated by the tile-like structures around the origin in Fig. 3.

III. PHOTON-VARIED QUANTUM STATES

Techniques involving photon addition (or subtraction) to squeezed-vacuum states have been effectively utilized to generate Schrödinger cat states [32–35] and can also produce multi-component cat states [30, 49], highlighting the benefits of multi-photon operations. In our current work, we use photon addition and subtraction operations on quantum states to create innovative nonclassical quantum states. These newly proposed states could potentially align with modern experimental setups, as discussed in [34, 35]. In the following sections, we present the quantum states that are the focus of our study, ac-

accompanied by a thorough theoretical investigation. This detailed analysis explores the phase-space characteristics and implications of these quantum states, providing a comprehensive understanding of their characteristics and significance.

A. Deformed Coherent States

Here, we examine the foundational concepts leading to our primary quantum states, specifically deformed coherent states [36–38]. These deformed coherent states are generated by applying a sequence of photon addition and subtraction, or vice versa, to a standard coherent state. We now explore how these operations modify the coherent state, resulting in the creation of deformed coherent states and their significance in our study.

The sequence of photon operations is crucial in our case, as different orders produce different results. Consider the scenario where p photons are first added to a state followed by the subtraction of q photons. This sequence appears as subtraction and addition (SA) operations, and is denoted appropriately for a coherent state as

$$|\oplus\rangle := N_{\oplus}^{-1/2} \hat{a}^q \hat{a}^{\dagger p} |\alpha\rangle, \quad (12)$$

where

$$N_{\oplus} = (-1)^{p+q} \sum_{n=0}^p \Gamma H_{p-n,q} [i\alpha, i\alpha^*] \times H_{p-n,q} [i\alpha^*, i\alpha] \quad \text{with } \Gamma := \frac{(-1)^n (p!)^2}{n![(p-n)!]^2} \quad (13)$$

represents the normalization coefficient, and $H_{x,y}$ denotes the bivariate Hermite polynomial.

In the addition-subtraction (AS) scenario, the process involves first subtracting q photons from a state, followed with the addition of p photons. This sequence of operations, for a coherent state, can be denoted as

$$|\ominus\rangle := N_{\ominus}^{-1/2} \hat{a}^{\dagger p} \hat{a}^q |\alpha\rangle \quad (14)$$

with

$$N_{\ominus} = \sum_{n=0}^p (-1)^n \Gamma H_{p-n,q} [\alpha, \alpha^*] H_{p-n,q} [\alpha^*, \alpha] \quad (15)$$

denotes the normalization coefficient.

The Wigner functions of SA and AS cases are evaluated using Eq. (1). Compared to their counterparts of ordinary coherent states, these Wigner functions attain non-Gaussian form and may hold negative phase-space attributes for different values of p and q , highlighting their nonclassical nature [36].

First, for the SA example, the relevant Wigner function is derived as

$$W_{|\oplus\rangle}(\beta) = \frac{1}{N_{\oplus}} W_{|\alpha\rangle\langle\alpha|}(\beta) \sum_{n=0}^p \Gamma H_{p-n,q} [-i\Omega, -i\alpha^*] \times H_{p-n,q} [i\Omega^*, i\alpha] \quad \text{with } \Omega := 2\beta - \alpha. \quad (16)$$

The non-Gaussian nature of this Wigner function is obvious from the expression, and as it is also evident in Figs. 4(a)-(c) that this Wigner function now acquired negative amplitudes, suggesting the nonclassical nature of this state. Here, note that Fig. 4(a) with $p = 0$ and $q = 0$, presents the case of corresponding ordinary coherent state, but as observed in Figs. 4(b) and 4(c), when p grows, negative regions are amplified, while the q parameter has the opposite impact.

Mathematically, the Wigner function for the AS case has an analogous form to that of the SA case,

$$W_{|\ominus\rangle}(\beta) = \frac{1}{N_{\ominus}} W_{|\alpha\rangle\langle\alpha|}(\beta) \sum_{n=0}^p \Gamma H_{p-n,q} [\Omega^*, \alpha] \times H_{p-n,q} [\Omega, \alpha^*]. \quad (17)$$

This Wigner function is shown in Figs. 4(d)-(f) with different p and q values, indicating that the corresponding Wigner functions also contains negative amplitudes in the phase space. It is interesting to note that when q is applied directly on a coherent state, there is no effect, as shown in Fig. (4)(d) with $p = 0$ and $q = 2$ appearing to have the same Wigner function as a coherent state. As illustrated in Fig. (4)(e), similar to SA case, the photon addition in this case also enhances the negative regions. However, as can be observed in Fig. (4)(f), with a nonzero value of p , the parameter q appears to be effective and serves the same as in the previous SA example, that is, it appears to make the negative regions less dense. The effects of p and q on the phase space are more thoroughly discussed for the quantum states presented in the following sections.

To emphasize that, as presented in Fig. 4, it is clear that both SA and AS cases presented above are non-Gaussian, and the negativity in their Wigner functions confirms their nonclassical nature, which lacks in the original coherent states. The addition and subtraction (or subtraction and addition) of an equal number of photons from a quantum state can result in two different quantum states. This is confirmed here by two AS and SA cases of coherent states with equivalent photon operations resulting in distinct quantum states, as shown by their Wigner function graphs, and can also be confirmed by the non-commutativity of the bosonic operators \hat{a}^{\dagger} and \hat{a} .

B. Photon Statistics

The photon addition and subtraction operations, as examined in our case, are anticipated to affect the photon

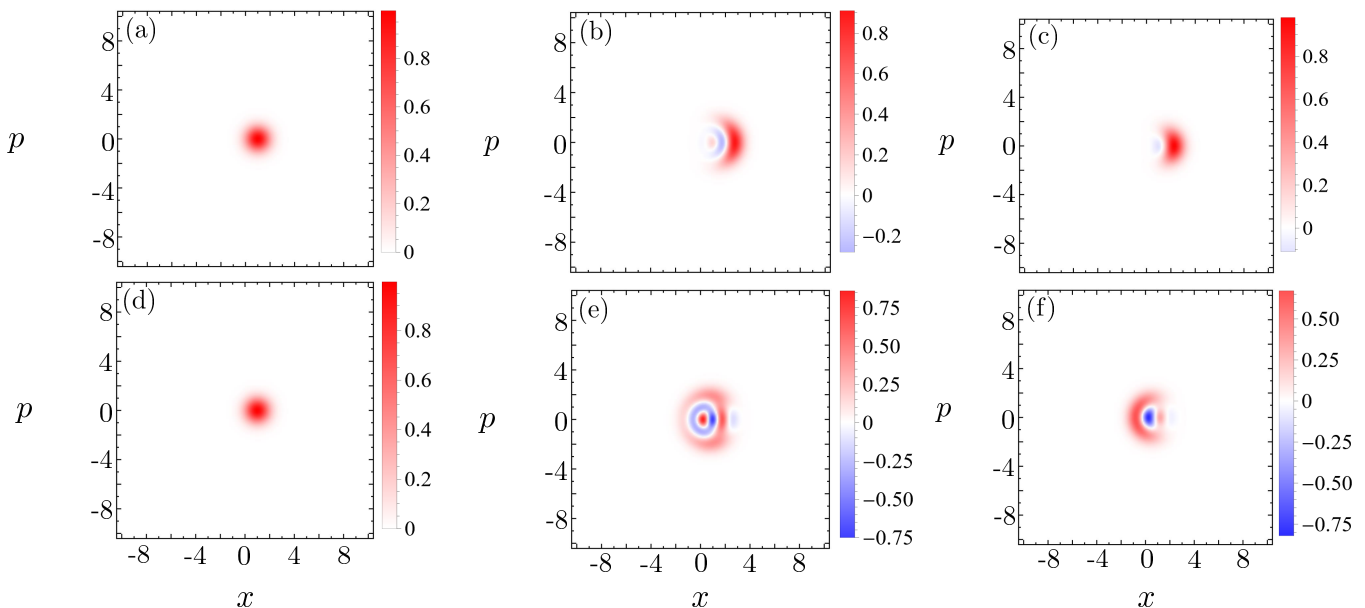


FIG. 4. (a)-(c) represents Wigner distributions of the SA case of a coherent state, and (d)-(f) represents the corresponding AS cases: (a) $p = 0$, $q = 0$; (b) $p = 4$, $q = 2$; (c) $p = 4$, $q = 4$; (d) $p = 0$, $q = 2$; (e) $p = 4$, $q = 2$; and (f) $p = 4$, $q = 4$.

number distribution (PND) of our quantum states. For example, in the compass state, the sizes of sub-Planck structures, phase-space sensitivity, and PND are all proportional to the macroscopic parameter. We now illustrate the effects of multi-photon operations on the photon statistics of resulting deformed coherent states. To investigate the PND in these SA and AS scenarios of the coherent state, we use the mathematical expression for PND of a quantum state $|\psi\rangle$, denoted as $P_{|\psi\rangle}(n) := |\langle n|\psi\rangle|^2$, where $|n\rangle$ represents the Fock state [7].

The photon number distributions for the SA and AS cases, denoted as $P_{|\oplus\rangle}(n)$ and $P_{|\ominus\rangle}(n)$, are evaluated as follows:

$$P_{|\oplus\rangle}(n) = \frac{N_{\oplus}[(q+n)!]^2 \kappa}{n![(q+n-p)!]^2} \text{ and } P_{|\ominus\rangle}(n) = \frac{N_{\ominus} n! \kappa}{[(n-p)!]^2} \quad (18)$$

with

$$\kappa := |\alpha|^{2(q-p+n)} e^{-|\alpha|^2}. \quad (19)$$

Let us now analyze these distributions. Here, Figs. 5(a)-(c) show the PND for the SA case of the coherent state for different situations based on the varying amount of added and subtracted photons. As depicted in Fig. 5(a), PND with $p = 0$ and $q = 0$ exhibits a Poissonian distribution, which obviously corresponds to a coherent state. In Fig. 5(b), when $p = 4$ photons are added and set $q = 0$, the Poissonian distribution shifts to higher values of n , with the peak now occurring at a larger mean photon number. In Fig. 5(c), the Poissonian distribution shifts to lower values of n , as with an increment in the subtracting photons to $q = 4$, and the number of added

photons is kept at $p = 4$ as in the prior instance. These cases reflect that in the SA examples, a higher p corresponds to a higher average photon number, whereas a higher q corresponds to a lower average photon number in the resultant state.

The PND for AS case is shown in Figs. 5(d)-(f) with a few p and q values. As illustrated in Fig. 5(d), for $q = 2$ and $p = 0$, the statistics of PND stay constant, showing that raising the number of subtracted photons has no influence on the average photon number of the states when applied directly to a coherent state. As observed in Fig. 5(e), increasing the number of added photons while maintaining the number of subtracted photons constant, that is, with $p = 4$ and $q = 2$, drives the Poissonian distribution to a larger n . In Fig. 5(f), the number of subtracted photons is increased to $q = 4$ without changing p , and it is observed that subtracting photons from a coherent state has no influence on the related PND. This is an additional confirmation of how photon subtraction operations keep PND of this case invariant. Hence, photon addition in both the SA and AS situations increases the average photon number in the subsequent states; however, the AS case maintains the distribution at higher mean photon values, implying that this situation has higher average photon numbers than the SA case.

In the upcoming sections, we present and explore the SA and AS cases of the compass states. We provide a comprehensive analysis that builds on the foundational concepts introduced above. This detailed examination presents the discussion about the characteristics and implications of these specific cases, offering insights into their behavior and significance within the framework

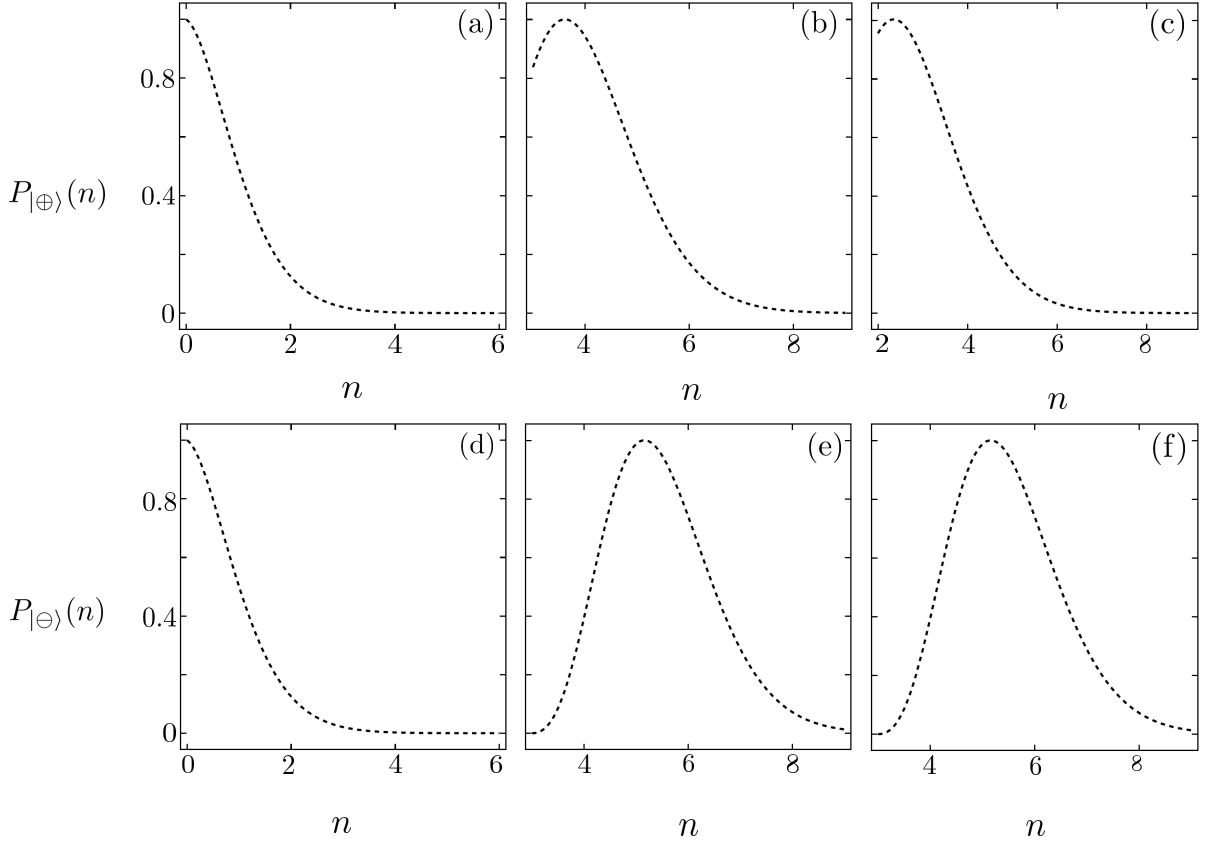


FIG. 5. PND for SA and AS cases are represented by $P_{|\oplus\rangle}(n)$ and $P_{|\ominus\rangle}(n)$, respectively. (a) $p = 0, q = 0$; (b) $p = 4, q = 2$; (c) $p = 4, q = 4$; (d) $p = 0, q = 2$; (e) $p = 4, q = 2$; and (f) $p = 4, q = 4$. We use $\alpha = 1/\sqrt{2}$ in all cases, and distributions are normalized to unity.

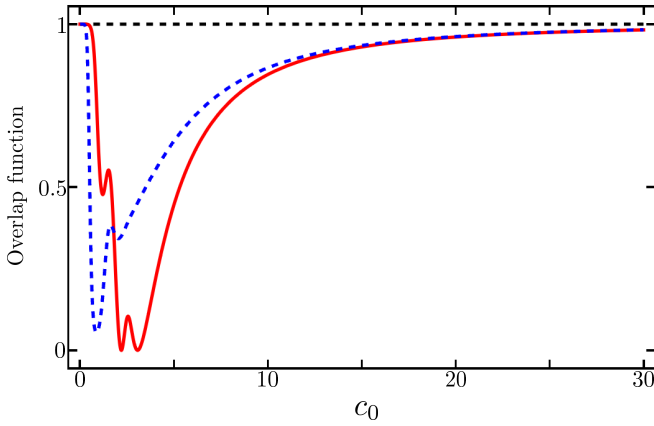


FIG. 6. The overlap function $|F_{\square}(c_0)|^2$ is represented as a blue dashed curve and $|F_{\blacksquare}(c_0)|^2$ as a red solid line, with $p = 4$ and $q = 4$. The horizontal black dashed line depicts the case where $p = 0$ and $q = 0$; consequently, the overlap is simply between two compass states.

of our study.

C. Variants of a Kitten State

In §III A, we noticed that the SA and AS variants of a standard coherent state exhibit fascinating phase-space properties that surpass those of the original coherent states. It is observed that the sequence in which photon operations are applied significantly affects the outcome, resulting in two distinct quantum states with different phase-space characteristics for the SA and AS cases. We now extend these concepts to other quantum states of interest in the sections that follow.

We now introduce SA and AS cases of our interest. For our SA scenario, p photons are added to the compass state $|\diamond\rangle$ as given in Eq. (5), followed by the subtraction of q photons. In the AS scenario, q photons are first subtracted from the compass state, and then p photons are added. These photon operations on the compass state produce new quantum states, which may display distinct phase-space characteristics.

The resulting SA case is denoted as $|\square\rangle$ and mathematically described as:

$$|\square\rangle := N_{\square}^{-1/2} \hat{a}^q \hat{a}^{\dagger p} \sum_{i=1}^4 |\alpha_i\rangle \quad (20)$$

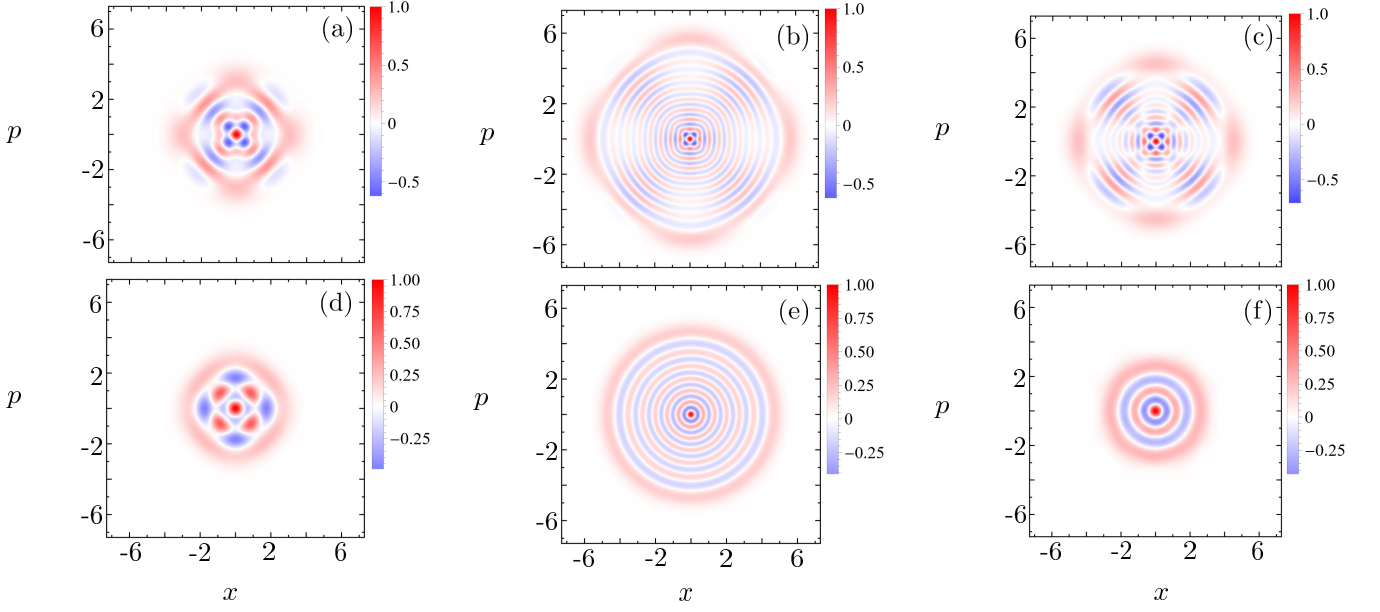


FIG. 7. (a)-(c) show the Wigner function of the SA case of the compass state, and (d)-(f) show the analogous AS cases. (a) $p = 12$, $q = 12$, (b) $p = 24$, $q = 12$, (c) $p = 24$, $q = 20$, (d) $p = 12$, $q = 12$, (e) $p = 24$, $q = 12$, and (f) $p = 24$, $q = 20$. In all cases, we set $c_0 = 1$.

with

$$N_{\square} = (-1)^{p+q} \sum_{i,j=1}^4 \Gamma G_{\alpha_i, \alpha_j} e^{\alpha_i^* \alpha_j} H_{p-n, q} [i\alpha_j, i\alpha_i^*] \times H_{p-n, q} [i\alpha_i^*, i\alpha_j] \quad (21)$$

denotes the normalization coefficient.

In the same way, the AS situation, denoted as $|\blacksquare\rangle$, is represented as follows:

$$|\blacksquare\rangle := N_{\blacksquare}^{-1/2} \hat{a}^{\dagger p} \hat{a}^q \sum_{i=1}^4 |\alpha_i\rangle, \quad (22)$$

where

$$N_{\blacksquare} = \sum_{i,j=1}^4 (-1)^n \Gamma G_{\alpha_i, \alpha_j} e^{\alpha_i^* \alpha_j} H_{p-n, q} [\alpha_j, \alpha_i^*] \times H_{p-n, q} [\alpha_i^*, \alpha_j] \quad (23)$$

represents the normalization factor for this case.

We now compare the original compass state with the proposed variants by assessing their overlap. This overlap indicates how distinct the proposed states are from the original compass state. By optimizing the parameters to maximize this distinction, we will analyze the characteristics of the states with these optimized parameters.

Let us evaluate the overlap between our SA case and the compass state. The overlap is represented by $F_{\square}(c_0) := \langle \square | \diamond \rangle$ and is calculated as

$$F_{\square}(c_0) = (-i)^{p+q} [N_{\square} N_{\diamond}]^{-1/2} \sum_{i,j=1}^4 F_{|\square_i\rangle \langle \square_j|} \quad (24)$$

with

$$F_{|\square_i\rangle \langle \square_j|} := G_{\alpha_i, \alpha_j} e^{\alpha_i^* \alpha_j} H_{p, q} [i\alpha_i^*, i\alpha_j], \quad (25)$$

and is depicted with a blue dashed line in Fig. 6.

Now, we provide the overlap between AS and compass state, which is denoted as $F_{\blacksquare}(c_0) := \langle \blacksquare | \diamond \rangle$. This overlap reads

$$F_{\blacksquare}(c_0) = [N_{\blacksquare} N_{\diamond}]^{-1/2} \sum_{i,j=1}^4 F_{|\blacksquare_i\rangle \langle \blacksquare_j|} \quad (26)$$

with

$$F_{|\blacksquare_i\rangle \langle \blacksquare_j|} := G_{\alpha_i, \alpha_j} e^{\alpha_i^* \alpha_j} H_{p, q} [\alpha_i^*, \alpha_j], \quad (27)$$

and is plotted with a red solid line in Fig. 6.

In Fig. 6, the black dashed line represents the overlap between two same compass states, and recalling that the parameter c_0 measures the mutual separation between the coherent states, as discussed in the §III B, this parameter has a strong impact on the characteristics of the original compass state, that is, the existence of the sub-Planck structures and enhanced sensitivity is associated with higher c_0 values. For example, the scenario represented in Fig. 1(a) for comparatively smaller c_0 does not have the capacity to exhibit these traits, and this particular case is named as four-headed kitten state.

Note that in our plots, we only investigated the overlaps for the $p = q = 4$ case, because it is understood here that for other higher values of p and q , our proposed states will hold more difference different than the compass state for smaller c_0 values, as depicted here; thus,

this result is meaningful for other settings of p and q . In these plots, it is clear that greater c_0 values cause the blue dashed and red solid lines to coincide with the horizontal dashed black line, suggesting that the respective SA and AS cases revived to the original compass state. However, when parameter c_0 is smaller, our proposed SA and AS cases diverge significantly from the original compass state, as illustrated in the plot, where the blue dashed and red solid curves are much lower than the black horizontal dashed line.

In the following, we assume $c_0 = 1$ and then investigate the detailed phase-space characteristics of the associated four-headed cat state using varied photon addition and subtraction operations. Here, we simply refer to these consequent states as SA and AS cases of this kitten state, and our analysis is divided into the subsections follows. In §III D, we demonstrate and examine the phase-space characteristics of these quantum states. In §III E, we analyze the sensitivity to phase-space displacement for each example.

D. Analysis of Distinctive Phase-Space Features

To this point, we have introduced the SA and AS cases of our interest, each producing distinct quantum states. In these instances, photon addition and subtraction processes appeared to have a main impact on their characteristics, and in this section, we particularly employ the Wigner function to investigate the corresponding phase space of these quantum states. To obtain the Wigner function for each case, Eq. (1) is employed, and we denote $W_{|\square\rangle}(\beta)$ and $W_{|\blacksquare\rangle}(\beta)$ as the corresponding Wigner functions of SA and AS cases of the kitten state, respectively.

Let us now examine the Wigner distributions for each scenario. For the SA case of our kitten state introduced in Eq. (20), the Wigner distribution is calculated as follows:

$$W_{|\square\rangle}(\beta) = \frac{1}{N_{\square}} \sum_{i,j=1}^4 W_{|\square_i\rangle\langle\square_j|}(\beta), \quad (28)$$

where

$$W_{|\square_i\rangle\langle\square_j|}(\beta) := W_{|\alpha_i\rangle\langle\alpha_j|}(\beta) \sum_{n=0}^p \Gamma H_{p-n,q} [i\Omega_j^*, i\alpha_i] \times H_{p-n,q} [-i\Omega_i, -i\alpha_j^*] \quad (29)$$

with

$$\Omega_{\mu} := 2\beta - \alpha_{\mu}. \quad (30)$$

In the same way, for the AS situation depicted in Eq. (22), we have

$$W_{|\blacksquare\rangle}(\beta) = \frac{1}{N_{\blacksquare}} \sum_{i,j=1}^4 W_{|\blacksquare_i\rangle\langle\blacksquare_j|}(\beta), \quad (31)$$

where

$$W_{|\blacksquare_i\rangle\langle\blacksquare_j|}(\beta) := W_{|\alpha_i\rangle\langle\alpha_j|}(\beta) \sum_{n=0}^p \Gamma H_{p-n,q} [\Omega_j^*, \alpha_i] \times H_{p-n,q} [\Omega_i, \alpha_j^*]. \quad (32)$$

The relevant Wigner functions are presented in Fig. 7, with Fig. 8 illustrating the central phase-space features of each case, where for both figures the cases labelled with (a)-(c) exhibit the SA, while (d)-(f) provides equivalent AS cases of the kitten state. It is readily apparent that our SA and AS instances achieve substantially distinct phase-space characteristics. Interestingly, a central sub-Planck structure is identified in each of the cases outlined. We focus on the significance of the sub-Planck structure in these states and examine this particular phase-space feature in detail.

Photons addition and subtraction appeared to have a significant effects in the Wigner distribution of the corresponding states. Note that the the original compass states, represented in Fig. 1(a) with $c_0 = 1$, do not exhibit a sub-Planck structure. As we stated before, this particular situation is also known as a kitten state. This implies that appearance of the sub-Planck structures in our cases is attributed to the photon operations involved. Specifically, it is observed that as the parameter p , which represents the number of added photons, increases, the size of sub-Planck structure reduces uniformly in both the SA and AS cases. This is evident by comparing the scenarios presented in Figs. 8(a) and 8(b) for the SA case, and then Figs. 8(d) and 8(e) is for corresponding AS cases, where increasing p with constant q , clearly depicts this impact. We have already noticed in §III A that photons subtraction operation applied to a coherent state has no effects in the phase space, but when combined with the photons addition operation, this operation has also the significant effects, that is, an increase in the parameter q denoting the number of photons subtractions causes to reduce the size of the sub-Planck structure, as observed in Figs. 8(b) and 8(c) for the SA case and then Figs. 8(e) and 8(f) are representing this impact for the AS cases.

A notable change in the sub-Planck structures is observed when transitioning from the Zurek compass state to the SA and AS cases, that is, some of these cases display nearly isotropic sub-Planck structures resemble to those of the compass state, whereas others, especially as shown in Figs. 8(e) and 8(f), are quite isotropic. The isotropic behavior of these cases is clearly evident, as demonstrated by the circular structure around the origin. This indicates that, for these scenarios, the sub-Planck structure is uniformly constrained in all directions of the phase space. Note that our variants for $q = 0$ are simply photon-added kitten states, as it is understood that such states may also exhibit similar phase-space features, whereas the case when $p = 0$ is irrelevant to the current discussion because the ineffectiveness of the parameter q without parameter p is obvious from the discussion.

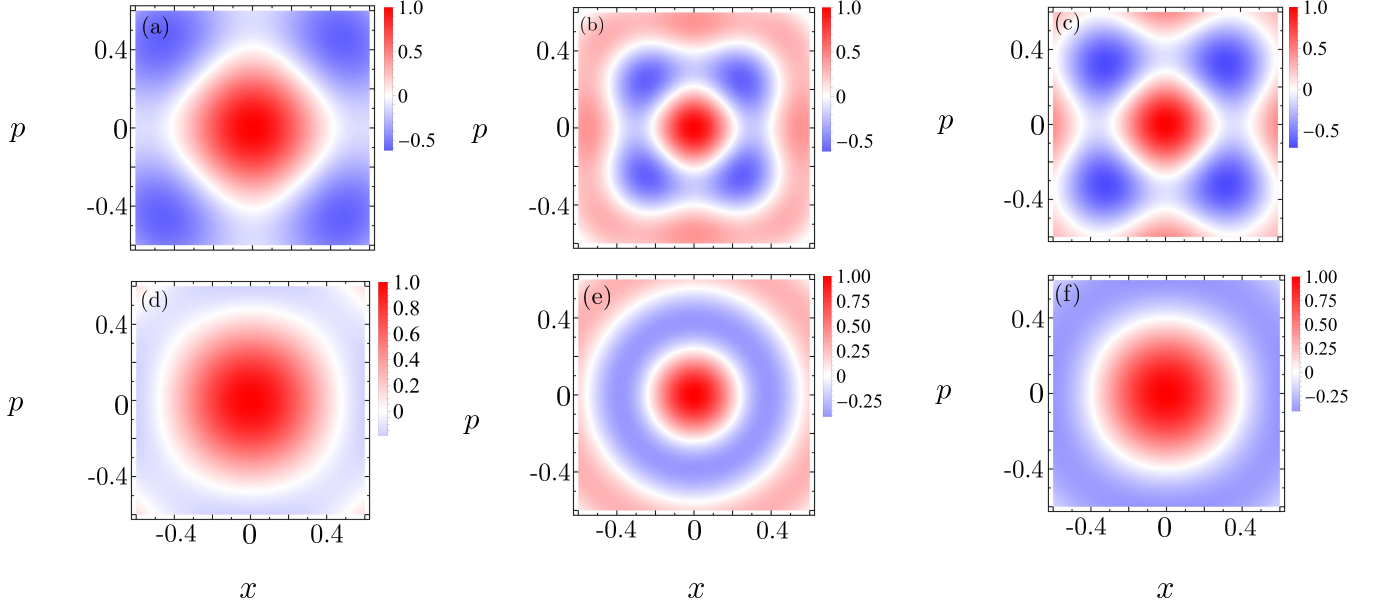


FIG. 8. The central phase-space structures of the cases depicted in Fig. 7. (a) $p = 12$, $q = 12$, (b) $p = 24$, $q = 12$, (c) $p = 24$, $q = 20$, (d) $p = 12$, $q = 12$, (e) $p = 24$, $q = 12$, and (f) $p = 24$, $q = 20$. In all cases, we set $c_0 = 1$.

Furthermore, the SA and AS cases with differing average photon numbers, with the AS example having a higher average photon number, appear to exhibit distinct sub-Planck structures, demonstrated by the associated phase space intensity figures.

In summary, photon addition and subtraction in a smaller compass state, also referred to as a four-component (or four-headed) kitten state, result in a significantly larger compasslike state that maintains a sub-Planck structure in its phase space. Interestingly, this transition from the compass state to our states has the advantage of making the ensuing sub-Planck structures isotropic in some situations. Our variants may also exhibit comparable metrological capacity as the compass state, which we will explore in the next section by analyzing their sensitivity to phase-space displacement.

E. Enhancement in Sensitivity

Sensitivity and its relationship to the phase-space characteristics of a quantum state are thoroughly discussed in the §II A. This concept is then applied to the compass state in the §II B, where it is demonstrated that the presence of sub-Planck structures in those states significantly have enhanced their sensitivity to displacement and that optimizing controlling parameters may further enhance this sensitivity far better than the standard quantum limit. In §III D, we thoroughly examined the phase space of the proposed SA and AS cases, confirming the presence of sub-Planck structures in their phase spaces. We will now examine how these sub-Planck structures have impact on the sensitivity to phase-space displacement,

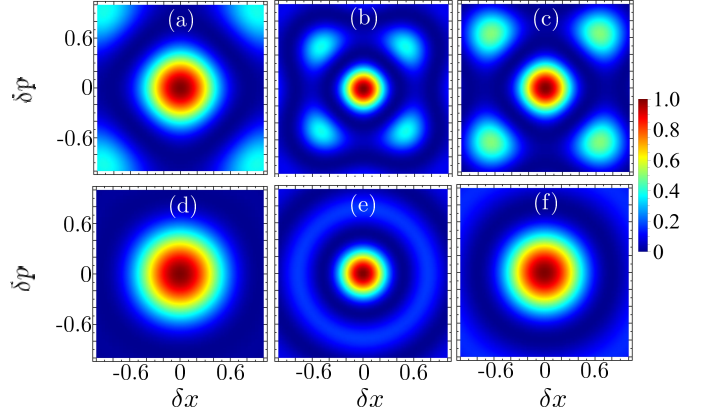


FIG. 9. Overlap between a state and its slightly translated version with (a)-(c) depict SA examples, whereas (d)-(f) exhibit comparable AS cases: (a) $p = 12$, $q = 12$, (b) $p = 24$, $q = 12$, (c) $p = 24$, $q = 20$, (d) $p = 12$, $q = 12$, (e) $p = 24$, $q = 12$, and (f) $p = 24$, $q = 20$. In all situations, we set $c_0 = 1$ and normalize the intensity plots to unity.

which is analyzed by assessing the sensitivities using Eq. (3).

First, for the SA scenario, we denote the associated sensitivity as $S_{|\square\rangle}(\delta)$, and is calculated as

$$S_{|\square\rangle}(\delta) = \left| \sum_{i,j=1}^4 O_{|\square_i\rangle|\square_j\rangle}(\delta) \right|^2 \quad (33)$$

with

$$O_{|\square_i\rangle\langle\square_j|}(\delta) := G_{\alpha_i, \alpha_j} \Lambda \sum_{n=0}^p (-1)^n \Gamma H_{p-n, q} [i(\alpha_i^* - \delta^*), i\alpha_j] \\ \times H_{p-n, q} [-i(\alpha_j + \delta), -i\alpha_i^*] \quad (34)$$

and

$$\Lambda := \exp \left[-\alpha_j \delta^* - \frac{|\delta|^2}{2} + \alpha_i^* \alpha_j + \alpha_i^* \delta \right]. \quad (35)$$

In the AS situation, the sensitivity $S_{|\blacksquare\rangle}(\delta)$ is found as

$$S_{|\blacksquare\rangle}(\delta) = \left| \sum_{i, j=1}^4 O_{|\blacksquare_i\rangle\langle\blacksquare_j|}(\delta) \right|^2, \quad (36)$$

where

$$O_{|\blacksquare_i\rangle\langle\blacksquare_j|}(\delta) := G_{\alpha_i, \alpha_j} \Lambda \sum_{n=0}^p (-1)^n \Gamma H_{p-n, q} [\alpha_i^* - \delta^*, \alpha_j] \\ \times H_{p-n, q} [\alpha_j + \delta, \alpha_i^*]. \quad (37)$$

The corresponding sensitivities $S_{|\square\rangle}(\delta)$ and $S_{|\blacksquare\rangle}(\delta)$ with $\delta := (\delta x + i\delta p)/\sqrt{2}$ are shown in the Figs. 8(a)-(c) and Figs. 8(d)-(f), respectively.

Let us now examine the SA case presented in the Figs. 8(a)-(c), where it is evident that the overlap is zero for values of $|\delta| < 1$ along any direction in phase space. This indicates that the sensitivity to displacement in this scenario surpasses the standard limit. The enhancement in sensitivity becomes more pronounced as the parameter p , which represents the number of added photons to the kitten state, increases. As shown in Figs. 8(a) and 8(b), this effect becomes clearly noticeable with a higher number of added photons. Specifically, the central structure is significantly reduced when the number of added photons increases from $p = 12$ to $p = 24$ with the number of subtracted photons, $q = 12$, remains constant in this situation. Furthermore, the impact of increasing the number of eliminated photons from $q = 12$ to $q = 20$ is illustrated in the Figs. 8(b) and 8(c), where an enlargement in the central structure occurs, indicating that a higher value of $|\delta|$ relative to the earlier case represented in Fig. 8(b) is needed to make the overlap zero. This suggests that the sensitivity to displacement in this circumstance decreases as q grows; hence, contrary to p , increasing the number of subtracted photons reduces sensitivity in the SA scenario.

In the AS instance, as illustrated in Figs. 8(d)-(f), similar to the SA case, an improved sensitivity to phase space displacements δ is noticed, and the values $|\delta| < 1$ can render the $S_{|\blacksquare\rangle}(\delta)$ zero as observable by the central structure. Similar to the SA example, this amplification becomes more noticeable as p increases, as illustrated in the instances depicted in Figs. 8(d) and 8(e), and then when q is increased, the improvement in the sensitivity is reduced. Isotropic regions, such as the circles centered

at the origin shown in Figs. 8(d) and 8(e), indicates that in the AS case, sensitivity is uniformly enhanced in all directions.

In summary, in this section, we introduced an extensive examination of our proposed SA and AS cases of a kitten state, examined their phase space, and argued that such states offer sub-Planck structures that differ from a compass state in certain cases. Also it is suggested that the sensitivity in both SA and AS scenarios is significantly lower than the norm. In the next section, we present a full analysis of these results in relation to previous results, including brief physical explanations, implications, and beyond.

IV. DISCUSSION AND REMARKS

We now provide an overview of our findings by discussing their physical consequences and comparing them to previous research in the subject. This comprehensive discussion strives to integrate our findings into current understanding, providing a detailed picture of their effects and contributions to the field.

The original compass state considered as a main example in our study [17], and our investigations and discussion are centered around this distinctive catlike state, which serves as the foundation for our exploration and examination. The compass state exhibits fascinating sub-Planck scale structures and enhanced sensitivity. However, these characteristics are lost when transitioning to a kitten state [34], which is essentially a smaller version of the cat state. This transition occurs when the macroscopic parameter is reduced, resulting in a shift from a cat state to a kitten state. Specifically, a bigger compass state exhibits pronounced sub-Planck features, indicating more refined quantum characteristics at scales lower than the Planck length; as discussed in §II B and then depicted in Fig. 1. Furthermore, the mean photon number in a bigger compass state is higher, indicating enhanced total photon content and intensity. This comparison demonstrates the significant differences in quantum behavior and measurement precision between the larger compass and kitten states; as observed in Fig. 3.

Photon addition and subtraction operations on squeezed-vacuum states are extremely useful approaches for creating larger cat states [32–35]. These methods have been demonstrated experimentally and provide an effective way to generate cat states of larger amplitude [34, 35]. In this study, we utilized the kitten version of the compass state and applied photon addition and subtraction operations with different order and magnitudes to construct our novel variants, as presented in Fig. 7. We then investigated the phase-space characteristics of these variants to gain insights into their quantum properties. The kitten version of the compass state, as shown in Fig. 1(a), which does not possess sub-Planckness, is now transformed into the states holding sub-Planck structures and demonstrating an en-

hanced sensitivity, implying the effectiveness of these multi-photon processes, as evident in Fig. 8 and Fig. 9. When the number of photons added increases, nonclassical features contained by these states are improved, but increasing photon subtraction destroys nonclassical structures in phase space. Note that this only occurs when the photon subtraction operation is combined with addition; otherwise, when photon subtraction is applied to a coherent state directly, the phase space remains unchanged [see Fig. 4]. Furthermore, photon addition raises the average photon count in the states, whereas photon subtraction maintains the photon statistics invariant.

This indicates that our states exhibit comparable phase-space attributes as the compass state when there are increased number of photon addition is performed. The photon subtraction plays an opposite role but we observed in our case their presence is also important. That is, in some cases the sub-Planck structures exhibited by our variants have isotropic form, as illustrated in Figs. 8(e) and 8(f). Furthermore, these variants have demonstrated a similar isotropic enhancement in sensitivity, as shown in Figs. 9(e) and 9(f). Except that with an appropriate photon subtractions the phase-space characteristics of our quantum states can also be controlled. This implies that our variants are an appropriate substitute to compass states, may be closely related to the current experiments, and can perform better under optimum conditions. Compasslike states built by superposition of compass states have also built isotropic forms of the sub-Planck structures [51], but our variants are obtained and followed a complete different technique, and presenting a completely different form in which photon addition and subtraction plays the main role in occurring of these intriguing characteristics. Also, note that the intricate su-

perposition of higher number of quantum states can also be difficult to achieve in experiments. For example, as demonstrated in [14], coherent-state superpositions can be generated via third-order Kerr nonlinearity, which is relatively challenging to accomplish in experiments. Furthermore, catlike states are highly susceptible to loss, and because absorption cannot be ignored in currently available Kerr media, the capacity to extract coherent-state superposition before they fragile is severely limited [63], hence, comparatively, adding and subtracting photons from a quantum state is a better technique to construct such states [34, 35].

In conclusion, we presented an alternative versions of a compass state that exhibits sub-Planck structures and has an increased sensitivity than quasi-classical states (such as coherent states), making it suitable for quantum metrology applications. Our two variations achieved distinct properties, and in certain situations they perform better as compared to a compass state. Hence, our quantum states could serve as a reliable alternatives for these compass states. Further research is required to explore how to create these variants, which will require a novel and thorough investigation to develop new techniques for their generation. This endeavor will involve formulating innovative strategies and methodologies specifically designed to produce these advanced quantum states.

ACKNOWLEDGEMENT

This work is supported by the Natural Science Foundation of Jiangsu Province (Grant No. BK20231320) and the National Natural Science Foundation of China (Grant No. 12174157).

-
- [1] E. Schrödinger, Der stetige übergang von der mikro- zur makromechanik, *Sci. Nat.* **14**, 664 (1926).
 - [2] P. W. Milonni and M. M. Nieto, Coherent states, in *Compendium of Quantum Physics*, (Springer, Berlin, Heidelberg, 2009).
 - [3] R. J. Glauber, Coherent and incoherent states of the radiation field, *Phys. Rev.* **131**, 2766 (1963).
 - [4] C. Gerry and P. Knight, *Introductory Quantum Optics* (Cambridge University Press, England, Cambridge, 2005).
 - [5] V. Bužek and P. L. Knight, *Quantum Interference, Superposition States of Light and Nonclassical Effects*, Prog. Opt., Vol. 34 (Elsevier, Amsterdam, 1995) p. 1.
 - [6] E. Wigner, On the quantum correction for thermodynamic equilibrium, *Phys. Rev.* **40**, 749 (1932).
 - [7] W. P. Schleich, *Quantum Optics in Phase Space* (Wiley-VCH, Weinheim, 2001).
 - [8] J. Joo, W. J. Munro, and T. P. Spiller, Quantum metrology with entangled coherent states, *Phys. Rev. Lett.* **107**, 083601 (2011).
 - [9] P. Walther, J.-W. Pan, M. Aspelmeyer, R. Ursin, S. Gasparoni, and A. Zeilinger, De Broglie wavelength of a non-local four-photon state, *Nature* **429**, 158 (2004).
 - [10] M. W. Mitchell, J. S. Lundeen, and A. M. Steinberg, Super-resolving phase measurements with a multiphoton entangled state, *Nature* **429**, 161 (2004).
 - [11] K. Johnson, J. Wong-Campos, B. Neyenhuis, J. Mizrahi, and C. Monroe, Ultrafast creation of large Schrödinger cat states of an atom, *Nat. Commun.* **8**, 697 (2017).
 - [12] A. Facon, E.-K. Dietsche, D. Grosso, S. Haroche, J.-M. Raimond, M. Brune, and S. Gleyzes, A sensitive electrometer based on a Rydberg atom in a Schrödinger-cat state, *Nature* **535**, 262 (2016).
 - [13] G. J. Milburn, Quantum and classical Liouville dynamics of the anharmonic oscillator, *Phys. Rev. A* **33**, 674 (1986).
 - [14] B. Yurke and D. Stoler, Generating Quantum Mechanical Superpositions of Macroscopically Distinguishable States via Amplitude Dispersion, *Phys. Rev. Lett.* **57**, 13 (1986).
 - [15] N. Shukla, N. Akhtar, and B. C. Sanders, Quantum tetrachotomous states: Superposition of four coherent states on a line in phase space, *Phys. Rev. A* **99**, 063813 (2019).
 - [16] L. A. Howard, T. J. Weinhold, F. Shahandeh, J. Combes, M. R. Vanner, A. G. White, and M. Ringbauer, Quantum

- hypercube states, *Phys. Rev. Lett.* **123**, 020402 (2019).
- [17] W. H. Zurek, Sub-Planck structure in phase space and its relevance for quantum decoherence, *Nature* **412**, 712 (2001).
- [18] U. Leonhardt, *Measuring the Quantum State of Light*, Vol. 22 (Cambridge university press, Cambridge, England, 1997).
- [19] H. P. Robertson, The uncertainty principle, *Phys. Rev.* **34**, 163 (1929).
- [20] D. A. R. Dalvit, R. L. de Matos Filho, and F. Toscano, Quantum metrology at the Heisenberg limit with ion trap motional compass states, *New J. Phys.* **8**, 276 (2006).
- [21] F. Toscano, D. A. R. Dalvit, L. Davidovich, and W. H. Zurek, Sub-Planck phase-space structures and Heisenberg-limited measurements, *Phys. Rev. A* **73**, 023803 (2006).
- [22] S. L. Braunstein and P. van Loock, Quantum information with continuous variables, *Rev. Mod. Phys.* **77**, 513 (2005).
- [23] G. S. Agarwal and P. K. Pathak, Mesoscopic superposition of states with sub-Planck structures in phase space, *Phys. Rev. A* **70**, 053813 (2004).
- [24] P. K. Pathak and G. S. Agarwal, Generation of a superposition of multiple mesoscopic states of radiation in a resonant cavity, *Phys. Rev. A* **71**, 043823 (2005).
- [25] Z. Leghtas, G. Kirchmair, B. Vlastakis, M. H. Devoret, R. J. Schoelkopf, and M. Mirrahimi, Deterministic protocol for mapping a qubit to coherent state superpositions in a cavity, *Phys. Rev. A* **87**, 042315 (2013).
- [26] L. C. G. Govia, E. J. Pritchett, and F. K. Wilhelm, Generating nonclassical states from classical radiation by subtraction measurements, *New J. Phys.* **16**, 045011 (2014).
- [27] N. Ofek, A. Petrenko, R. Heeres, P. Reinhold, Z. Leghtas, B. Vlastakis, Y. Liu, L. Frunzio, S. M. Girvin, L. Jiang, M. Mirrahimi, M. H. Devoret, and R. J. Schoelkopf, Extending the lifetime of a quantum bit with error correction in superconducting circuits, *Nature* **536**, 441 (2016).
- [28] B. Vlastakis, G. Kirchmair, Z. Leghtas, S. E. Nigg, L. Frunzio, S. M. Girvin, M. Mirrahimi, M. H. Devoret, and R. J. Schoelkopf, Deterministically encoding quantum information using 100-photon Schrödinger cat states, *Science* **342**, 607 (2013).
- [29] L. Praxmeyer, C.-C. Chen, P. Yang, S. D. Yang, and R. K. Lee, Direct measurement of time-frequency analogs of sub-Planck structures, *Phys. Rev. A* **93**, 053835 (2016).
- [30] G. B. Lemos, R. M. Gomes, S. P. Walborn, P. H. S. Ribeiro, and F. Toscano, Experimental observation of quantum chaos in a beam of light, *Nat. Commun.* **3**, 2041 (2012).
- [31] J. Wenger, R. Tualle-Brouri, and P. Grangier, Non-gaussian statistics from individual pulses of squeezed light, *Phys. Rev. Lett.* **92**, 153601 (2004).
- [32] M. Dakna, T. Anhut, T. Opatrny, L. Knöll, and D.-G. Welsch, Generating Schrödinger-cat-like states by means of conditional measurements on a beam splitter, *Phys. Rev. A* **55**, 3184 (1997).
- [33] X.-B. Tang, F. Gao, Y.-X. Wang, J.-G. Wu, and F. Shuang, Non-Gaussian features from excited squeezed vacuum state, *Opt. Commun.* **345**, 86 (2015).
- [34] A. Ourjoumteev, R. Tualle-Brouri, J. Laurat, and P. Grangier, Generating optical Schrödinger kittens for quantum information processing, *Science* **312**, 83 (2006).
- [35] J. S. Neergaard-Nielsen, B. M. Nielsen, C. Hettich, K. Mølmer, and E. S. Polzik, Generation of a superposition of odd photon number states for quantum information networks, *Phys. Rev. Lett.* **97**, 083604 (2006).
- [36] Z. Wang, H. chun Yuan, and H. yi Fan, Nonclassicality of the photon addition-then-subtraction coherent state and its decoherence in the photon-loss channel, *J. Opt. Soc. Am. B* **28**, 1964 (2011).
- [37] S. M. Barnett, G. Ferenczi, C. R. Gilson, and F. C. Speirits, Statistics of photon-subtracted and photon-added states, *Phys. Rev. A* **98**, 013809 (2018).
- [38] S. Guerrini, M. Z. Win, and A. Conti, Photon-varied quantum states: Unified characterization, *Phys. Rev. A* **108**, 022425 (2023).
- [39] P. Jacquod, I. Adagideli, and C. W. J. Beenakker, Decay of the Loschmidt Echo for Quantum States with Sub-Planck-scale Structures, *Phys. Rev. Lett.* **89**, 154103 (2002).
- [40] D. A. Wisniacki, Short-time decay of the Loschmidt echo, *Phys. Rev. E* **67**, 016205 (2003).
- [41] S. Ghosh, A. Chiruvelli, J. Banerji, and P. K. Panigrahi, Mesoscopic superposition and sub-Planck-scale structure in molecular wave packets, *Phys. Rev. A* **73**, 013411 (2006).
- [42] L. Praxmeyer, P. Wasylczyk, C. Radzewicz, and K. Wódkiewicz, Time-Frequency Domain Analogues of Phase Space Sub-Planck Structures, *Phys. Rev. Lett.* **98**, 063901 (2007).
- [43] J. R. Bhatt, P. K. Panigrahi, and M. Vyas, Entanglement-induced sub-Planck phase-space structures, *Phys. Rev. A* **78**, 034101 (2008).
- [44] M. Stobińska, G. J. Milburn, and K. Wódkiewicz, Wigner function evolution of quantum states in the presence of self-Kerr interaction, *Phys. Rev. A* **78**, 013810 (2008).
- [45] S. Ghosh, U. Roy, C. Genes, and D. Vitali, Sub-Planck-scale structures in a vibrating molecule in the presence of decoherence, *Phys. Rev. A* **79**, 052104 (2009).
- [46] U. Roy, S. Ghosh, P. K. Panigrahi, and D. Vitali, Sub-Planck-scale structures in the Pöschl-teller potential and their sensitivity to perturbations, *Phys. Rev. A* **80**, 052115 (2009).
- [47] N. Akhtar, B. C. Sanders, and C. Navarrete-Benlloch, Sub-Planck structures: Analogies between the Heisenberg-Weyl and SU(2) groups, *Phys. Rev. A* **103**, 053711 (2021).
- [48] N. Akhtar, B. C. Sanders, and G. Xianlong, Sub-Planck phase-space structure and sensitivity for SU(1,1) compass states, *Phys. Rev. A* **106**, 043704 (2022).
- [49] N. Akhtar, J. Wu, J.-X. Peng, W.-M. Liu, and G. Xianlong, Sub-Planck structures and sensitivity of the superposed photon-added or photon-subtracted squeezed vacuum states, *Phys. Rev. A* **107**, 052614 (2023).
- [50] N. Akhtar, X. Yang, M. Asjad, J.-X. Peng, G. Xianlong, and Y. Chen, Compasslike states in a thermal reservoir and fragility of their nonclassical features, *Phys. Rev. A* **109**, 053718 (2024).
- [51] A. Shukla and B. C. Sanders, Superposing compass states for asymptotic isotropic sub-Planck phase-space sensitivity, *Phys. Rev. A* **108**, 043719 (2023).
- [52] K. M. R. Audenaert, Comparisons between quantum state distinguishability measures, *Quantum Inf. Comput.* **14**, 31 (2014).
- [53] D. Dieks, Overlap and distinguishability of quantum states, *Phys. Lett. A* **126**, 303 (1988).

- [54] C. Navarrete-Benlloch, *An Introduction to the Formalism of Quantum Information with Continuous Variables* (Morgan & Claypool/IOP, Bristol, 2015).
- [55] J.-P. Gazeau, *Coherent States in Quantum Physics* (Wiley-VCH, Berlin, 2009).
- [56] J. Weinbub and D. K. Ferry, Recent advances in wigner function approaches, *Appl. Phys. Rev.* **5**, 041104 (2018).
- [57] H. Yi Fan and H. Zaidi, Application of IWOP technique to the generalized Weyl correspondence, *Phys. Lett. A* **124**, 303 (1987).
- [58] V. Dodonov, I. Malkin, and V. Man'ko, Even and odd coherent states and excitations of a singular oscillator, *Physica* **72**, 597 (1974).
- [59] C. Song, K. Xu, H. Li, Y.-R. Zhang, X. Zhang, W. Liu, Q. Guo, Z. Wang, W. Ren, J. Hao, H. Feng, H. Fan, D. Zheng, D.-W. Wang, H. Wang, and S.-Y. Zhu, Generation of multicomponent atomic Schrödinger cat states of up to 20 qubits, *Science* **365**, 574 (2019).
- [60] J. Hastrup, J. S. Neergaard-Nielsen, and U. L. Andersen, Deterministic generation of a four-component optical cat state, *Opt. Lett.* **45**, 640 (2020).
- [61] Su-Yong Lee, Chang-Woo Lee, Hyunchul Nha, and Dagomir Kaszlikowski, Quantum phase estimation using a multi-headed cat state, *J. Opt. Soc. Am. B* **32**, 1186 (2015).
- [62] G. S. Thekkadath, B. A. Bell, I. A. Walmsley, and A. I. Lvovsky, Engineering Schrödinger cat states with a photonic even-parity detector, *Quantum* **4**, 239 (2020).
- [63] R. W. Boyd, Order-of-magnitude estimates of the nonlinear optical susceptibility, *J. Mod. Opt.* **46**, 367 (1999).